Original Research Article

Quantum state estimation of a qubit using adaptive measurements

Nattima Thong-O[1], Tosaporn Angsachon[1] and Atirach Ritboon[1,2,*]

[1]Department of Physics, Faculty of Science and Technology, Thammasat University, Khlong Nueng, Khlong Luang, Pathum Thani, 12120, Thailand

[2]Research Unit in Energy Innovations and Modern Physics (EIMP), Thammasat University, Khlong Nueng, Khlong Luang, Pathum Thani, 12120, Thailand

[*]Corresponding author E-mail: ritboon@tu.ac.th

Received: 11th September 2025, Revised: 28th December 2025, Accepted: 30th December 2025

Abstract

Quantum state estimation is one of the most extensively studied topics in the field of quantum theory and quantum information. This process is essential in quantum protocols to ensure that the estimated state matches the true state. Typically, the quantum state of identical systems can be estimated from the statistics of measurement outcomes across different measurement bases. In this research, we study adaptive-measurement strategies for quantum state estimation used to identify a pure state of two-level systems and compare the obtained estimated state to the state obtained when the measurement bases are chosen randomly. The adaptive measurements in this study include the maximum-information-gain strategy, and the confirmation strategy. In this work, we simulate the outcome of the measurement on a system and use the Bayesian estimation method to estimate the obtained state. We then adaptively change the basis of the next measurement in accordance with the estimated state and the used adaptive strategy. We find that the maximum-information-gain strategy provides the fastest convergence and the most accurate state estimation compared to the confirmation strategy and the randomly-chosen-measurement-basis strategy, especially in the presence of measurement noise.

Keywords: Quantum state estimation, State tomography, Adaptive measurements

Introduction

Quantum state estimation or quantum state tomography is the process of identifying an unknown state of identically prepared quantum systems through a series of measurements in different sets of bases. It is considered a cornerstone of quantum technology developments as it plays a central role in characterizing and verifying the properties of quantum systems [1,2], such as quantum coherence [3,4] and quantum entanglement [5-7]. It has been performed in various quantum platforms including trapped ions [5,8,9], optical systems [6,10], and superconducting circuits [7,11], leading to various applications in quantum optics, quantum information processing, and quantum communication. It allows us to verify the performance and functionality of quantum devices, operations, and protocols, ensuring that they are performed as expected both individually and collectively. The verification of quantum states and operations is even more essential in the fields of quantum metrology and quantum sensing as the measurement precision and sensitivity crucially depend on the efficiency in quantum state preparation of the probe [12] and on how its state changes during the sensing process [13,14]. Additionally, we note here that the required number of measurements and computational resources in determining the unknown quantum state grows exponentially with the size or the dimensionality of the quantum systems [15].

We may classify the types of state estimation in accordance with the structure of the Hilbert space of the system, including continuous-variable (CV) and discrete-variable state estimation. For continuous-variable state estimation in optics, the state of the system can be measured through homodyne or heterodyne detection, and the measurement outcomes can be used to reconstruct the Wigner function, or other characteristic functions, such as Q or P functions. For discrete-variable state estimation, which is the focus of this work, we may generally use the outcomes from projective measurements on the systems to estimate the state through linear inversion [16], maximum likelihood estimation [17], or Bayesian inference [18]. For example, we can construct a qubit state from a sequence of measurements in X, Y, and Z Pauli bases. For the state estimation of qubits, there have been several proposed adaptive measurement methods such as the adaptive quantum state estimation based on locally unbiased measurements and maximum likelihood estimation [19,20], adaptive state estimation using self-learning measurements [18] and symmetry measurements [21].

In this work, we would like to examine whether an adaptive measurement strategy, based on the self-learning protocol provided in [18], with a sufficiently simple measurement basis adjusting can improve the state estimation of a pure qubit state, especially in the presence of measurement noise. The protocol adopted the Bayesian inference method to update the probability density and estimate the quantum state based on the measurement outcomes. Once the estimated state is obtained, we adjust the measurement basis accordingly and repeat all the processes again. The results of the adaptive strategies are then compared to the results obtained via randomly chosen measurement bases, which is regarded as the benchmark.

Quantum state of an ensemble

We particularly focus on the state estimation of an ensemble in which there exists a finite number of particles prepared in an identical pure qubit state expressed as,

$$|\theta,\phi\rangle = \cos\left(\frac{\theta}{2}\right)|0\rangle + e^{i\phi}\sin\left(\frac{\theta}{2}\right)|1\rangle. \quad (1)$$

where θ and ϕ are the two angles representing the location of the pure state in the Bloch sphere. The corresponding density matrix of this pure state can be represented in the form of a Bloch vector $\vec{r}$ and the Pauli matrices as

$$\rho(\theta,\phi) = \frac{1}{2}(I + \vec{r}\cdot\vec{\sigma}) = \frac{1}{2}\left(I + r_x\sigma_x + r_y\sigma_y + r_z\sigma_z\right), \quad (2)$$

where $r_x = \sin\theta\cos\phi$, $r_y = \sin\theta\sin\phi$ and $r_z = \cos\theta$ are the Cartesian components of the Bloch vector.

To estimate the actual state $\rho(\theta,\phi)$, we, of course, need to perform measurements with different sets of measurement bases on the particles. Our key question here becomes how we can choose the basis of measurement in each measurement to make the estimation sufficiently converge to the state $\rho(\theta,\phi)$ of the ensemble within a finite number of measurements. For a sufficiently large ensemble, the simplest measurement strategy would be a randomly-chosen-measurement-basis strategy where the measurement is performed randomly. Once finishing the measurement process, one may use the sequence of measurement outcomes to estimate the state $\rho(\theta,\phi)$ of the ensemble. Adaptive measurement strategies, on the other hand, make use of the previous information of the preceding outcomes to adjust the measurement basis. As mentioned in the introduction, there have been several approaches of adaptive measurement developed so far and is proved to be successful in estimating a qubit state. In this research, however, we pose a simple question: if an adaptive approach with a straightforward measurement adjusting strategy can provide advantages in quantum state estimation of a qubit over the randomly-chosen-measurement-basis strategy, can such advantages still remain in the presence of measurement noises?

Suppose that the measurement basis is formed by two orthonormal projectors, which are

$$\begin{aligned}\hat{M}_0 &= \frac{1}{2}(I + \vec{m}\cdot\vec{\sigma}) = \frac{1}{2}\left(I + m_x\sigma_x + m_y\sigma_y + m_z\sigma_z\right),\\ \hat{M}_1 &= \frac{1}{2}(I - \vec{m}\cdot\vec{\sigma}) = \frac{1}{2}\left(I - m_x\sigma_x - m_y\sigma_y - m_z\sigma_z\right),\end{aligned} \quad (3)$$

where $\vec{m}$ is a unit vector of the Bloch sphere, i.e., $m_x^2 + m_y^2 + m_z^2 = 1$. In this basis, we associate the measurement outcomes 0 with the projector $\hat{M}_0$ and 1 with $\hat{M}_1$. The probability distribution in accordance with this measurement basis therefore can be explicitly written as

$$P\big(0|\rho(\theta,\phi)\big) = \mathrm{Tr}\left(\hat{M}_0\rho(\theta,\phi)\right) = \frac{1+\vec{r}\cdot\vec{m}}{2} = \frac{1+r_x m_x + r_y m_y + r_z m_z}{2} \tag{4}$$

$$P\big(1|\rho(\theta,\phi)\big) = \mathrm{Tr}\left(\hat{M}_1\rho(\theta,\phi)\right) = \frac{1-\vec{r}\cdot\vec{m}}{2} = \frac{1-\mathrm{r_x m_x} - \mathrm{r_y m_y} - \mathrm{r_z m_z}}{2} \tag{5}$$

where $P\big(i|\rho(\theta,\phi)\big)$ represents the probability of obtaining an outcome i when the ensemble is prepared in a state $\rho(\theta,\phi)$.

Measurement noises

Practically, the measurement process produces errors in measurement outcomes. Such errors may originate from different sources. For example, the detectors somehow cannot register all incoming signals due to their efficiency, and they sometimes can give false positives, regarded as dark counts. The errors may also originate from the imperfect measurement setting, such as the misalignment of an optical setup.

We suppose that the source of the noise means that the detector registers the wrong outcome of the qubit with a probability p and the correct outcome with the probability $1-p$. This means if the qubit is prepared in a pure state

$$\rho = \frac{1}{2}(I + \vec{m}\cdot\vec{\sigma}) = \frac{1}{2}\big(I + m_x\sigma_x + m_y\sigma_y + m_z\sigma_z\big), \tag{6}$$

where $\vec{m}$ is a unit vector, the measurement of the qubit along the direction $\vec{m}$ described by two projectors,

$$\begin{aligned}\hat{M}_0 &= \frac{1}{2}(I + \vec{m}\cdot\vec{\sigma}) = \frac{1}{2}\big(I + m_x\sigma_x + m_y\sigma_y + m_z\sigma_z\big),\\ \hat{M}_1 &= \frac{1}{2}(I - \vec{m}\cdot\vec{\sigma}) = \frac{1}{2}\big(I - m_x\sigma_x - m_y\sigma_y - m_z\sigma_z\big),\end{aligned} \tag{7}$$

would give the outcome 0 with probability $1-p$ and the outcome 1 with probability p respectively. To take the measurement noise into account, the probability distribution of the measurement outcomes described in Equations (4) and (5) will change into

$$
\begin{aligned}
P\big(0\big|\rho(\theta,\phi)\big) &= (1-p)\left(\frac{1+\vec{r}\cdot\vec{m}}{2}\right)+p\left(\frac{1-\vec{r}\cdot\vec{m}}{2}\right),\\
P\big(1\big|\rho(\theta,\phi)\big) &= (1-p)\left(\frac{1-\vec{r}\cdot\vec{m}}{2}\right)+p\left(\frac{1+\vec{r}\cdot\vec{m}}{2}\right),\\
&= 1-P\big(0\big|\rho(\theta,\phi)\big),
\end{aligned}
\tag{8}
$$

where again $P\big(i\big|\rho(\theta,\phi)\big)$ is the probability of obtaining a measurement outcome i when the qubit is ideally prepared in $\rho(\theta,\phi)$. The diagram representing the measurement noise is shown in Figure 1.

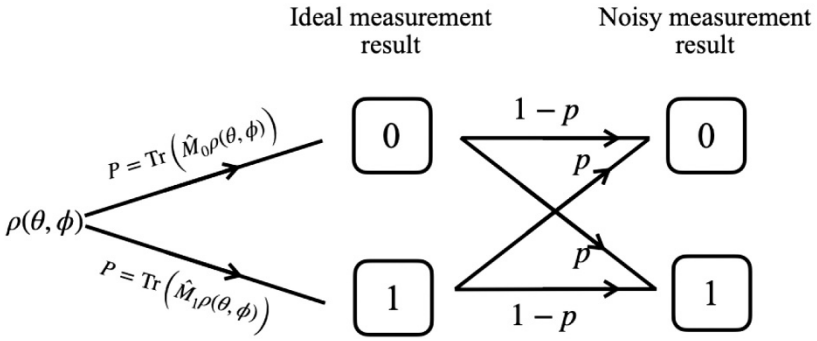

Figure 1 The probability tree diagram shows that the measurement readout is correctly registered with probability 1-p, whereas with probability p it arises from measurement error.

State estimation protocol

In this research, the estimation of the actual state $\rho(\theta,\phi)$ is achieved by updating the probability density in accordance with the measurement outcomes using Bayesian inference, as presented in [18]. The protocol of adaptive measurements includes only three main procedures.

1. We choose a measurement basis based on the priori information about the state obtained from the preceding measurement outcomes. We may randomly choose the initial measurement basis for the first measurement when no information about the actual state is yet available.

2. We perform a measurement in the chosen basis on a particle of the ensemble. Once the measurement outcome i is obtained, we update the probability distribution accordingly using Bayes' rule as

$$
P_n(\theta,\phi)=\frac{1}{Z_n}P\big(i\big|\rho(\theta,\phi)\big)P_{n-1}(\theta,\phi),
\tag{9}
$$

where $P_n(\theta,\phi)$ is the updated probability density after the nth round of the protocol, $P\left(i\middle|\rho(\theta,\phi)\right)$ is the probability associated with the outcome i of the measurement, given in Equation (8), $P_{n-1}(\theta,\phi)$ is the priori probability density, and Z_n is a normalization constant which is

$$Z_n = \int_0^{\pi} d\,\theta \sin\theta \int_0^{2\pi} d\,\phi P\left(i\middle|\rho(\theta,\phi)\right)P_{n-1}(\theta,\phi), \tag{10}$$

ensuring that the integration over θ and ϕ of $P_n(\theta,\phi)$ returns unity. For the first round where no priori information is yet available, these two angles can equally likely be any possible values, $0 \leq \theta \leq \pi$ and $0 \leq \phi \leq 2\pi$. As a result, the initial probability density of the parameters, in this case, is a constant

$$P_0(\theta,\phi) = \frac{1}{4\pi}. \tag{11}$$

3. Based on the updated probability distribution, the estimated state ρ_n using the outcome of the nth measurement can be given as

$$\rho_n = \frac{1}{2}(I + \vec{a}_n \cdot \vec{\sigma}) = \frac{1}{2}\left(I + a_{nx}\sigma_x + a_{ny}\sigma_y + a_{nz}\sigma_z\right), \tag{12}$$

where the components of the Bloch vector $\vec{a}_n$ are

$$a_{nx} = \int_0^{\pi} d\,\theta \sin\theta \int_0^{2\pi} d\,\phi \;\; P_n(\theta,\phi)\sin\theta\cos\phi\,, \tag{13}$$

$$a_{ny} = \int_0^{\pi} d\,\theta \sin\theta \int_0^{2\pi} d\,\phi \;\; P_n(\theta,\phi)\sin\theta\sin\phi\,, \tag{14}$$

$$a_{nz} = \int_0^{\pi} d\,\theta \sin\theta \int_0^{2\pi} d\,\phi \;\; P_n(\theta,\phi)\cos\theta\,, \tag{15}$$

We then repeat the first procedure by choosing the next basis measurement based on the obtained estimated state ρ_n.

We keep repeating these procedures until all particles are measured. The fidelity is used as a measure to quantify the proximity between the estimated state ρ_n and the actual state $\rho(\theta,\phi)$ of the ensemble, given by the scalar product of the two Bloch vectors $\vec{a}_n$ and $\vec{r}$ as

$$\mathcal{F} = \frac{1 + \vec{r}\cdot\vec{a}_n}{2}, \tag{16}$$

because the Bloch vector $\vec{r}$ is a unit vector. The closer the estimated state ρ_n is to the actual state $\rho(\theta,\phi)$ of the ensemble, the closer the fidelity approaches unity. Therefore, if the estimated state ρ_n does converge to the state $\rho(\theta,\phi)$ of the ensemble, their fidelity should approach unity when the number of measurements increases.

Measurement strategies

In this work, we only consider three different measurement strategies used for the state estimation from a finite number of measurements, including a randomly-chosen-measurement-basis strategy, a maximum-information-gain strategy, and a confirmation strategy. They are different in the way of choosing the measurement basis in each round, as discussed below.

1. The randomly-chosen-measurement-basis strategy

In this strategy, each measurement is performed with a random measurement basis in a way that all possible measurement bases are equally likely to be chosen. As the measurement basis is completely random, there is no information from the previous measurements that influences the choice of the subsequent measurement bases. It is obviously not an adaptive measurement, but it can serve as a reference to compare its results with the used adaptive measurements. The probability density, however, is updated as in Equation (9) each time we obtain the measurement outcome, and from the updated probability density, we can still estimate the actual state $\rho(\theta,\phi)$ using Equation (12).

2. The maximum-information-gain strategy

In this strategy, we choose the measurement basis in accordance with the estimated state ρ_n obtained from Equation (12). The measurement basis is chosen in such a way that the Bloch vector $\vec{m}$ of the projector $\hat{M}_i$ of the measurement basis is perpendicular to the vector $\vec{a}_{n-1}$ of the estimated state ρ_{n-1} of the previous measurement. For an even-numbered measurements and a given vector $\vec{a}_{n-1}$, the Gram-Schmidt process is used to determine a vector $\vec{m}$ as

$$\vec{m} = \frac{\vec{a}_{n-1} - (\vec{a}_{n-1}\cdot\vec{s})\vec{s}}{|\vec{a}_{n-1} - (\vec{a}_{n-1}\cdot\vec{s})\vec{s}|}, \tag{17}$$

where $\vec{s}$ is a random unit vector that is unparallel to the vector $\vec{a}_{n-1}$. The explicit form of the projectors associated with this Bloch vector $\vec{m}$ is given in Equation (3). For an odd-numbered measurement, the perpendicular Bloch vector $\vec{m}'$ is determined by the cross product between the vector $\vec{m}$ of the previous odd-numbered measurement and the Bloch vector $\vec{a}_{n-1}$ of the estimated state, given by

$$\vec{m}' = \vec{m} \times \vec{a}_{n-1} \tag{18}$$

We alternate the choice of measurement basis to ensure that the information extracted from the measurement outcomes is symmetric, as outcomes are obtained from both the measurements bases along the direction $\vec{m}$ and its perpendicular direction $\vec{m}'$. In this way, we expect the estimated state to converge symmetrically to the actual state $\rho(\theta, \phi)$ as the number of measurement increases.

As the actual state is unknown in an actual experiment, it is only the estimated probability distribution based on the obtained state ρ_{n-1} that can be accessed. As the Bloch vectors $\vec{m}$ and $\vec{m}'$ of the projectors in even- and odd-numbered measurements are both assigned to be perpendicular to the Bloch vector $\vec{a}_{n-1}$ of the estimated state ρ_{n-1}, the estimated probability distribution is then given by

$$P_0 = \mathrm{Tr}\left(\hat{M}_{0\rho_{n-1}}\right) = \frac{1 + \vec{a}_{\mathrm{n}-1} \cdot \vec{m}_k}{2} = \frac{1}{2}, \tag{19}$$

$$P_1 = \mathrm{Tr}\left(\hat{M}_{1\rho_{n-1}}\right) = \frac{1 - \vec{a}_{\mathrm{n}-1} \cdot \vec{m}_k}{2} = \frac{1}{2}, \tag{20}$$

where P_i represents the probability associated with the outcome i of the measurement and $\vec{m}_k$ is either the Bloch vector $\vec{m}$ or $\vec{m}'$. The estimated average information obtained from each measurement then becomes

$$S = -\sum_i P_i \ln P_i = 1 \tag{21}$$

As unity is the maximum of the estimated average information, this strategy is then called the maximum-information-gain, which was proposed as adaptive and self-learning measurements in [18]. In short, this work employs a slightly modified version of the strategy in Ref. [18] in which each set of two consecutive measurements is performed along two perpendicular axes, $\vec{m}$ and $\vec{m}'$, on the Bloch sphere.

3. The confirmation strategy

In contrast to the maximum-information-gain strategy, in this strategy we choose the measurement basis such that the unit Bloch vector $\vec{m}$ of the measurement basis is parallel to the Bloch vector $\vec{a}_{n-1}$ of the estimated state ρ_{n-1}, which is

$$\vec{m} = \frac{\vec{a}_{n-1}}{|\vec{a}_{n-1}|}, \tag{22}$$

so that this Bloch vector would approximately point in the same direction as that of the actual state $\rho(\theta,\phi)$, if $\rho_{n-1} \approx \rho(\theta,\phi)$. This means each measurement is performed to confirm the degree of directional alignment between the Bloch vector $\vec{a}_{n-1}$ of the estimated state ρ_{n-1} and that of the actual state $\rho(\theta,\phi)$.

Simulation results and discussion

We simulate 200 ensembles of different initial states $\rho(\theta,\phi)$. Each ensemble contains 300 identical qubits. We then simulate the measurement outcomes and update the probability density in accordance with Bayes' rule as discussed previously. The measurement basis of each measurement is then adjusted in accordance with the employed strategies. The results of the simulations are given in Figures 2.

The figure demonstrates the convergence of the average fidelity $\mathcal{F}$ between the actual states $\rho(\theta,\phi)$ of the ensembles the estimated states ρ_n using randomly-chosen-measurement-basis, maximum-information-gain, and confirmation strategies to unity after a sequence of measurements. The red, green, brown, and purple lines represent the average fidelity $\mathcal{F}$ with the probability of incorrect measurement readout of $p = 0.05$, $p = 0.10$, $p = 0.15$, and $p = 0.20$ respectively, while the blue dotted line is the fidelity for the noiseless case, $p = 0.00$. The shaded areas in different colors represent the regions in which the probability density of finding a simulated fidelity greater than 0.2. They are depicted in light blue, red, green, brown, and purple for the noise values of $p = 0.00$, $p = 0.05$, $p = 0.10$, $p = 0.15$, and $p = 0.20$ respectively. These areas stack on top of each other, making some of them hidden beneath others. For example, there is also a part of the light purple area that is hidden behind the other areas in Figure 2(a) and 2(b). These shaded areas can provide a sense of how the simulated fidelities are distributed around their average values.

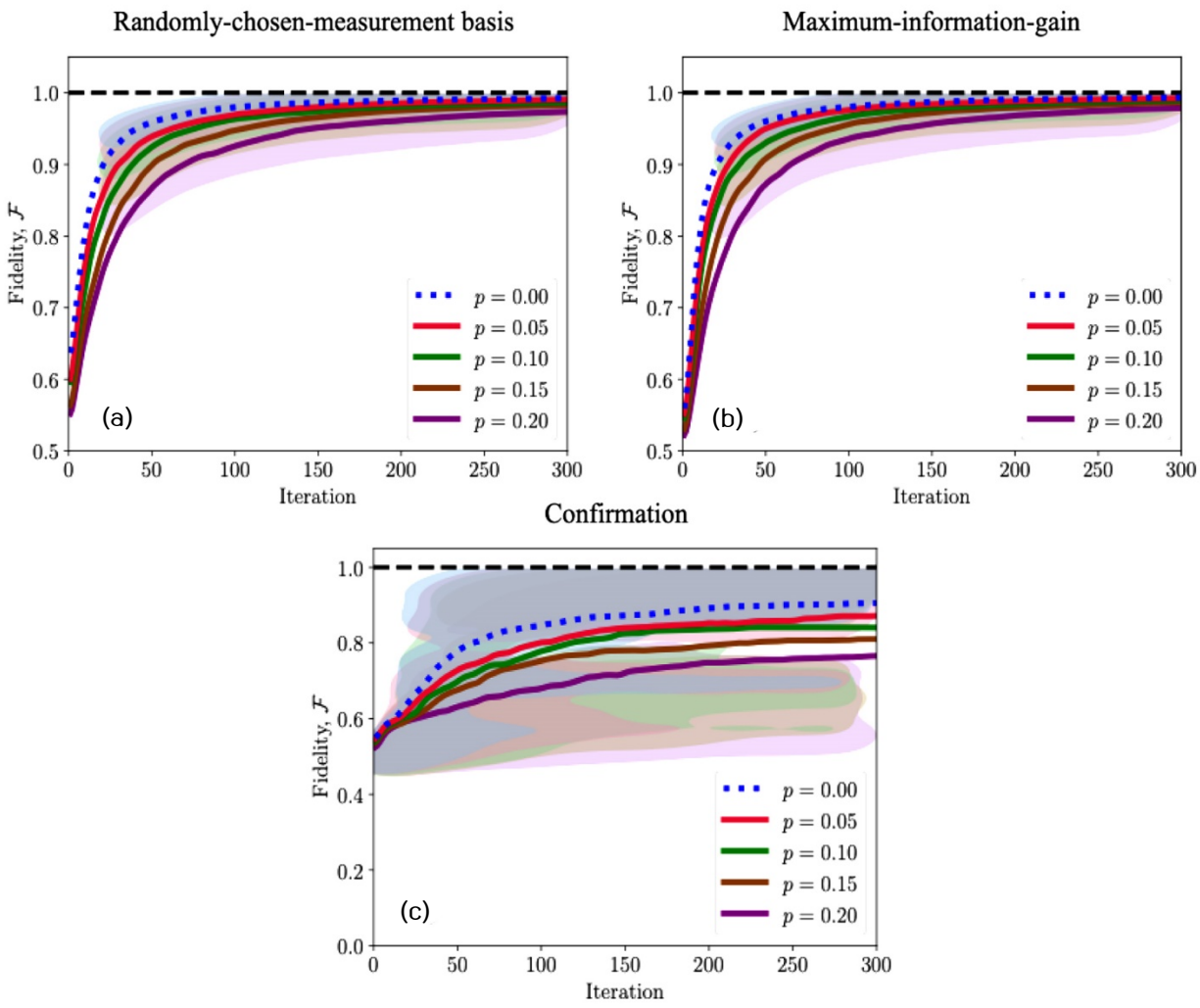

Figure 2 The simulated fidelity obtained from; (a) The randomly-chosen-measurement basis, (b) Maximum-information-gain, and (c) Confirmation strategies approach unity when the number of measurements increases. The red, green, brown and purple solid lines represent average fidelity obtained with different noise values: $p = 0.05$, $p = 0.10$, $p = 0.15$, *and* $p = 0.20$ *respectively, while that of the noiseless case is illustrated by the blue dotted line. We shade the areas in which the probability of finding a simulated fidelity greater than* 0.2 *in different colors for different noise values: light purple for* $\mathrm{p} = 0.20$, *light brown for* $\mathrm{p} = 0.15$, *light green for* $\mathrm{p} = 0.10$, *light red for* $\mathrm{p} = 0.05$ *and blue for the noiseless case. These areas can roughly illustrate the distribution of the simulated fidelities.*

It is apparent from the graphs that the measurement noise delays the convergence of the average fidelity. Moreover, the average fidelity obtained from the confirmation strategy noticeably lower than that from randomly-chosen-measurement-basis and maximum-information-gain strategies. This is because the way this strategy adjusts the measurement basis results in limited variation of

the measurement basis for estimating the actual state, see more details in the appendix. The statistics of the measurement using this strategy thus provide significantly lower information about the actual state $\rho(\theta,\phi)$ compared to the others. This also implies that the way we adjust the measurement basis in an adaptive measurement does affect the rate of convergence of the estimated state ρ_n.

We use the results of the randomly-chosen-measurement-basis strategy as the benchmark. Figure 3(a) demonstrates the difference of the average fidelities obtained from the maximum-information-gain and randomly-chosen-measurement-basis strategies in different values of measurement noise. It appears that the fidelity from the maximum-information-gain strategy is higher than that from the randomly-chosen-measurement basis, especially in the presence of measurement noise. This indicates that this adaptive measurement can enhance the convergence of the estimated state to the actual state when the number of measurements is sufficiently large. Their differences become more distinct at higher values of the measurement noise as the brown and purple lines are apparently higher than others after a sufficiently large number of iterations of measurements. This is due to the measurement outcomes from the maximum-information-gain strategy changing the probability density $P_n(\theta,\phi)$ in a subtle way such that unlikely outcomes caused by the noise does not significantly change the probability density $P_n(\theta,\phi)$. A wrong piece of information does not much deviate the estimation from the right track. Figure 3(b), on the other hand, illustrates the difference between the average fidelities obtained from the confirmation and randomly-chosen-measurement-basis strategies. The average fidelities of the confirmation strategy are lower than those of the randomly-chosen-measurement-basis strategy as reflected by the negativity of all curves in Figure 3(b). In addition, from the figure, as the noise level increases, the performance of the confirmation strategy deteriorates relative to the benchmark. This implies that this strategy is more prone to measurement errors compared to the benchmark.

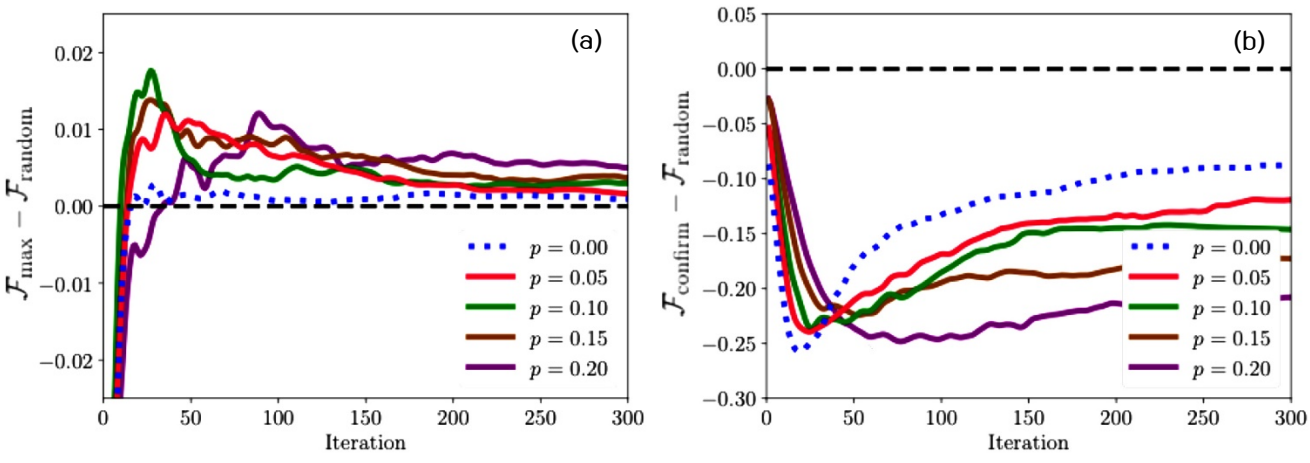

Figure 3 *Variation This figure shows; (a) The difference between the average fidelities obtained from the maximum-information-gain and randomly-chosen-measurement-basis strategies and (b) The*

difference between the average fidelities using the confirmation and randomly-chosen-measurement-basis strategies. Red, green, brown, and purple lines are used to display these differences when the noise is of values $p = 0.05$, $p = 0.10$, $p = 0.15$, *and* $p = 0.20$ *respectively, while that of the noiseless case is illustrated by the blue dotted line.*

Conclusion

We have simulated a state estimation protocol using two adaptive measurements, including the maximum-information-gain strategy and the confirmation strategy, and compared their results with the randomly-chosen-measurement-basis strategy used as a benchmark. As a result, the maximum-information-gain strategy can provide better state estimation than the randomly-chosen-measurement-basis strategy, especially in the presence of measurement noise. This is because this adaptive strategy progressively changes the probability density $P_n(\theta, \phi)$ in the most subtle way compared to other strategies. Measurement errors caused by the noise, therefore, cannot alter the probability density significantly. The confirmation strategy, on the other hand, provides the lowest performance. It turns out that this strategy limits the variation of the measurement bases, resulting in the slowest convergence of the state estimation.

Acknowledgment

AR acknowledges funding support from Thammasat University Research Unit in Energy Innovations and Modern Physics (EIMP).

References

[1] D. Gross, Y. Liu, and S. T. Flammia, S. Becker and J. Eisert, "Quantum state tomography via compressed sensing", Physical Review Letters, 105, 150401 (2010). https://doi.org/10.1103/PhysRevLett.105.150401.

[2] Y. Li, S. Ghosh, J. Shang, Q. Xiong and X. Zhang, "Estimating many properties of a quantum state via quantum reservoir processing", Physical Review Research, 6, 013211 (2024). https://doi.org/10.1103/PhysRevResearch.6.013211.

[3] D. Leibfried, D. M. Meekhof, C. Monroe, B. E. King, W. M. Itano and D. J. Wineland, "Experimental preparation and measurement of quantum states of motion of a trapped atom", Journal of Modern Optics, 44, 2485-2505 (1997).

[4] Z. Ding, R. Liu, C. Radhakrishnan, W. Ma, X. Peng, Y. Wang, T. Byrnes, F. Shi and J. Du, "Experimental study of quantum coherence decomposition and trade-off relations in a tripartite system", npj quantum information, 7, 145 (2021). https://doi.org/10.1038/s41534-021-00485-0.

[5] J. P. Home, M. J. McDonnell, D. M. Lucas, G. Imreh, B. C. Keitch, D. J. Szwer, N. R. Thomas, S. C. Webster, D. N. Stacey and A. M. Steane, "Deterministic entanglement and tomography of ion-spin qubits", New Journal of Physics, 8, 188 (2006). https://doi.org/10.1088/1367-2630/8/9/188.

[6] L. A. Rozema, C. Wang, D. H. Mahler, A. Hayat, A. M. Steinberg, J. E. Sipe and M. Liscidini, "Characterizing an entangled-photon source with classical detectors and measurements", Optica 2, 430-433 (2015). https://doi.org/10.1364/OPTICA.2.000430.

[7] C-K Hu, C. Wei, C. Liu, L. Che, Y. Zhou, G. Xie, H. Qin, G. Hu, H. Yuan, R. Zhou, S. Liu, D. Tan, T. Xin and D. Yu, "Experimental sample efficient quantum state tomography via parallel measurements", Physical Review Letters, 133, 160801 (2024). https://doi.org/10.1103/PhysRevLett.133.160801.

[8] H. Häffner, W. Hänsel, C. F. Roos, J. Benhelm, D. C. Kar, M. Chwalla, T. Körber, U. D. Rapol, M. Riebe, P. O. Schmidt, C. Becher, O. Gühne, W. Dür and R. Blatt, "Scalable multiparticle entanglement of trapped ions", Nature 438, 643-646 (2005). https://doi.org/10.1038/nature04279.

[9] C. Flühmann and J. P. Home, "Direct characteristic-fucntion tomography of quantum states of the trapped-ion motional oscillator", Physical Review Letters, 125, 043602 (2020). https://doi.org/10.1103/PhysRevLett.125.043602.

[10] J. L. O'Brien, G. J. Pryde, A. G. White, T. C. Ralph and D. Branning, "Demonstation of an all-optical quantum controlled-NOT gate", Nature, 426, 264-267 (2003). https://doi.org/10.1038/nature02054.

[11] A. S. Aasen, A. D. Giovanni, H. Rotzinger, A. V. Ustinov and M. Gärttner, "Readout error mitigated quantum state tomography tested on superconducting qubits", Communications Physics, 7, 301 (2024). https://doi.org/10.1038/s42005-024-01790-8.

[12] A. Farooq, U. Khalid, J. Rehman and H. Shin, "Robust quantum state tomography method for quantum sensing", Sensors, 22, 2669 (2022). https://doi.org/10.3390/s22072669.

[13] F. J. Schreiber, J. Eisert and J. J. Meyer, "Tomography of parametrized quantum states", PRX Quantum, 6, 020346 (2025). https://doi.org/10.1103/PRXQuantum.6.020346.

[14] E. O. Kiktenko, D. N. Kublikova and A. K. Fedorov, "Estimating the precision for quantum process tomography", Optical Engineering, 59, 061614 (2020). https://doi.org/10.1117/1.OE.59.6.061614.

[15] M. Cramer, M. B. Plenio, S. T. Flammia, R. Somma, D. Gross, S. D. Bartlett, O. Landon-Cardinal, D. Poulin and Y-K Liu, "Efficient quantum state tomography", Nature Communications, 1, 149 (2010). https://doi.org/10.1038/ncomms1147.

[16] M. A. Nielsen and I. L. Chuang, "Quantum computation and quantum information", Cambridge university press (2010).

[17] D. F. V. James, P. G. Kwiat, W. J. Munro and A. G. White, "Measurement of qubits", Physical Review A, 64, 052312 (2001). https://doi.org/10.1103/PhysRevA.64.052312.

[18] D. G. Fischer, S. H. Kienle and M. Freyberger, "Quantum-state estimation by self-learning measurements", Physical Review A, 61, 032306 (2000). https://doi.org/10.1103/PhysRevA.61.032306.

[19] A. Fujiwara, "Strong consistency and asymptotic efficiency for adaptive quantum estimation problems", Journal of Physics A: Mathematical and General, 39, 12489 (2006). https://doi.org/10.1088/0305-4470/39/40/014.

[20] R. Okamoto, S. Oyama, K. Yamagata, A. Fujiwara and S. Takeuchi, "Experimental demonstration of adaptive quantum state estimation for single photonic qubits", Physical Review A, 96, 022124 (2017). https://doi.org/10.1103/PhysRevA.96.022124.

[21] C. J. Happ and M. Freyberger, "Adaptive estimation of qubits by symmetry measurements", Physical Review A, 78, 064303 (2008). https://doi.org/10.1103/PhysRevA.78.064303.

Supplementary Materials

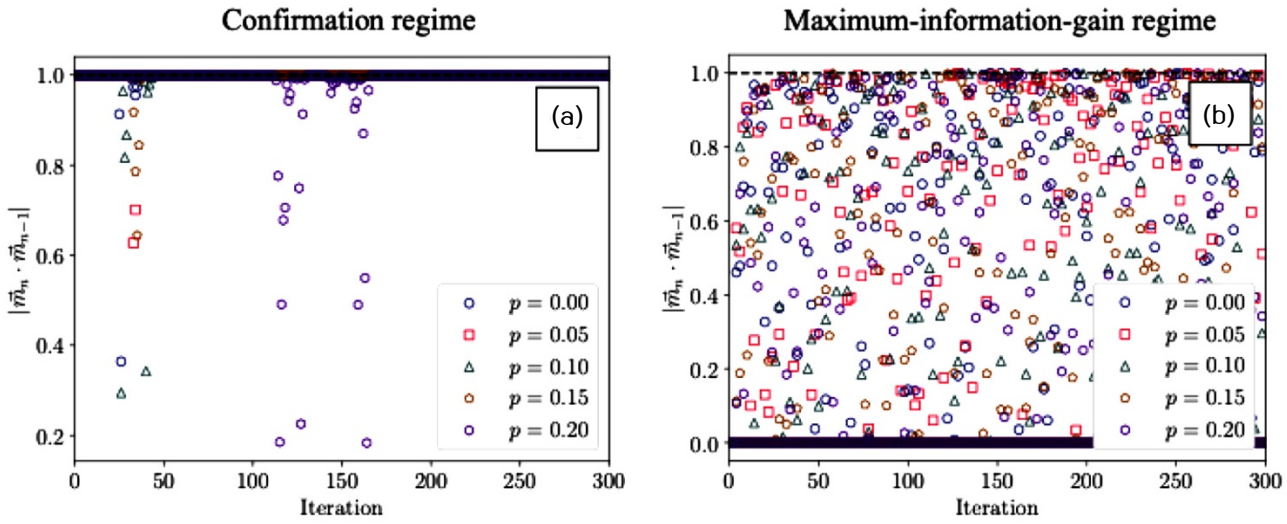

Figure S The figure illustrates the absolute value of the scalar product between the Bloch vectors $\vec{\mathrm{m}}_{\mathrm{n}}$ *and* $\vec{\mathrm{m}}_{\mathrm{n}-1}$ *of the projectors in the* n*th and* $(\mathrm{n}-1)$*th measurement bases using; (a) Confirmation and (b) Maximum-information-gain strategies. Circles, squares, triangles, pentagons, and hexagons represent the magnitudes of the scalar products when the noise is of values* $\mathrm{p} = 0.00$, $p = 0.05$, $p = 0.10$, $p = 0.15$, *and* $p = 0.20$ *respectively. Noticeably, most of them in Figure 4(a) is approximately unity reflecting the parallel of the Bloch vectors of the projectors implying that most of the time the confirmation strategy keeps selecting the same measurement basis.*

As we mentioned in the main text, the way we adjust the measurement bases in the confirmation strategy limits the variation of the used measurement bases in the protocol resulting in a slow convergence of the state estimation. Figure S displays the magnitudes of the scalar products between the Bloch vectors $\vec{\mathrm{m}}_{\mathrm{n}}$ and $\vec{\mathrm{m}}_{\mathrm{n}-1}$ of the projectors in the nth and $(\mathrm{n}-1)$th measurement bases using confirmation and maximum-information-gain strategies. Most of the magnitudes of the scalar products illustrated in Figure S(a) is approximately unity. This implies that most of the time the measurement bases employed in the confirmation strategy are nearly identical causing limited information about the actual state from the measurement outcomes and resulting in the slow convergence. In contrast, for the case of the maximum-information-gain strategy, the strategy uses relatively various measurement bases reflected by the scattered magnitudes of the scalar products of the Bloch vectors. Especially, as the odd-numbered measurements using the measurement bases with its projectors pointing in the perpendicular direction to that of the previous even-numbered measurements. This is why approximately half of the scalar products in Figure S(b) vanish.